DFG-Schwerpunktprogramm 1324

„Extraktion quantifizierbarer Information aus komplexen Systemen"

Function Spaces and Optimal Currents in Impedance Tomography

B. Jin, T. Khan, P. Maass, M. Pidcock

Preprint 17

DFG-Schwerpunktprogramm 1324

Function Spaces and Optimal Currents in Impedance Tomography

B. Jin, T. Khan, P. Maass, M. Pidcock

Preprint 17

The consecutive numbering of the publications is determined by their chronological order.

The aim of this preprint series is to make new research rapidly available for scientific discussion. Therefore, the responsibility for the contents is solely due to the authors. The publications will be distributed by the authors.

Function spaces and optimal currents in impedance tomography

Bangti Jin* Taufiquar Khan† Peter Maass* Michael Pidcock‡

June 11, 2009

Abstract

The main objective of this paper is to compare - analytically as well as numerically - different approaches for obtaining optimal input currents in impedance tomography. Following the approaches described in for example [13, 5, 12, 16], we aim at constructing input currents j, which contain the most information about the difference between the unknown physical conductivity σ^* and an estimate σ_0. The differences can be measured by different discrepancy functionals and the optimal input currents which maximize these functionals depend on the function spaces chosen for defining j and on the norm for measuring the discrepancy. Moreover, the definition of the appropriately weighted Sobolev spaces depends on σ and this subsequently influences the iteration for maximizing the functionals.

Numerical experiments illustrate features of the optimal input currents obtained for different combinations of function spaces. We compare the resulting optimal currents by a simplified sparse reconstruction algorithm.

1   Introduction

The electrical impedance tomography (EIT) problem is to determine a spatially varying electrical conductivity distribution σ within a bounded region $\Omega \subset \mathbb{R}^n (n = 2, 3)$ with a smooth boundary $\partial\Omega$ using electrical measurements made on the boundary. If we assume that σ is a strictly positive, isotropic and bounded conductivity distribution and that there are no current sources inside Ω, the basic mathematical model for the relevant EIT forward problem (σ known) is described by the elliptic differential equation for the electric potential u

$$- \operatorname{div} (\sigma \nabla u) = 0 \;\; \text{in } \Omega, \tag{1}$$

subject to the Neumann boundary condition $\sigma \frac{\partial u}{\partial n} = j$ on $\partial\Omega$.

An EIT data collection experiment consists of applying an electrical current (Neumann data) j on $\partial\Omega$ and measuring the resulting electrical potential (Dirichlet data) φ on $\partial\Omega$, thus giving some information on the Neumann-to-Dirichlet (NtD) map. In practise, a number of experiments using different input currents are made, and the inverse problem for EIT becomes that of determining an approximation to σ from a partial knowledge of the NtD map [6, 2, 19].

The optimal choice of the input current patterns in the experiment is important for any EIT reconstruction and several definitions of optimality, either function analytic [13, 12, 5, 9, 16] or statistical [14, 8], have been suggested. The function analytic approaches define optimality with respect to a discrepancy functional, which enables us to measure the difference between

---

*Center for Industrial Mathematics, University of Bremen, D-28334 Bremen, Germany (pmaass@math.uni-bremen.de).

†Department of Mathematical Sciences, Clemson University, Clemson, SC 29634-0975, USA.

‡Department of Mathematical Sciences, Oxford Brookes University, Oxford OX33 1HX, UK.

the true physical but unknown σ^* and an estimate σ_0. For an input current j, denote by φ^* the outcome of an EIT experiment, i.e. the Dirichlet data of the solution of (1), with $\sigma = \sigma^*$. We use the same input current j and denote by φ_0 the simulated Dirichlet data of the solution of (1) with $\sigma = \sigma_0$. We can then calculate the difference $\|\varphi^* - \varphi_0\|$ and define the optimal current by solving

$$\max_{j, \|j\|=1} \|\varphi^* - \varphi_0\|.$$

This approach was introduced in [13] for a setting with L_2-norms, and it was later formalized and mathematically justified in [10] as an eigenvalue problem. Similarly, the role of constraints, either pointwise or in the L_2-sense, in determining input currents and the associated optimization problems has been discussed in [17, 18]. Alternatively, we may use the approach of [16], which takes φ^* as input to a Dirichlet problem with $\sigma = \sigma_0$ and compares the resulting solution u^* with the solution u_0 of the Neumann problem with conductivity σ_0 and input current j. The optimal j is then obtained by maximizing

$$\max_{j, \|j\|=1} \|u^* - u_0\|.$$

In either case the optimal currents depend on the chosen norms for defining these discrepancy functionals as well as for measuring the input currents themselves. A first attempt in this direction was made in [5]. It starts by describing discrepancy functionals in different norms followed by a discussion of the influence of the chosen norms on the resulting optimal currents. However, after an introductory statement this paper returns to numerical investigations in the L_2-setting. A second attempt was made in [15, 16], where a functional comparing the solutions in the domain was proposed, but no numerical results were presented. Our more general approach will also overcome a certain lapse in the approach of [15, 16] which does not consider the dependence on σ of the chosen H^1-norms.

In summary, we aim at an analytic investigation of the influence of the norms of the function spaces on the resulting optimal currents. We will investigate different natural combinations of Sobolev and L_2- spaces and analyze the resulting optimal currents. The choice of the Sobolev spaces is justified by either the analytic properties of Neumann and Dirichlet problems, which suggests measuring the boundary data as well as the solution in Sobolev norms, or by physical considerations related to the dissipation power of EIT experiments, see [5]. The choice of the L_2-norms is justified by either modelling measurement errors or simply by numerical convenience. The results will be illustrated by numerical experiments. Consequently, we will obtain optimal currents for each discrepancy functional and we need a second criterion for differentiating between them. In Section 6 we will use a simplified sparse reconstruction procedure which determines an update for σ_0 based on a thresholded gradient step (shrinkage operation, line search).

The paper is organized as follows. In the next section we will review the formal analytic setting of EIT and define relevant function spaces. Section 3 contains the definition of the operators and in Section 4 we determine the associated adjoint operators. In Section 5 we derive the iteration procedure for obtaining optimal input currents based on these discrepancy functionals. Finally, Section 6 presents numerical experiments evaluating the optimality criteria.

2 Definitions and function spaces

We define the following Neumann and Dirichlet boundary value problems

$$
\begin{aligned}
-\operatorname{div}(\sigma \nabla u) &= 0 && \text{in } \Omega, \\
\sigma \tfrac{\partial u}{\partial n} &= j && \text{on } \partial \Omega,
\end{aligned}
\tag{2}
$$

and

$$
\begin{aligned}
-\operatorname{div}(\sigma \nabla u) &= 0 && \text{in } \Omega, \\
u &= \varphi && \text{on } \partial \Omega.
\end{aligned}
\tag{3}
$$

The conductivity σ is assumed to be bounded below and above, i.e. $0 < c_1 \le \sigma \le c_2 < \infty$. In addition, denote by $\gamma_D u$ the Dirichlet trace operator, i.e. the restriction of u to the boundary

$$
\begin{aligned}
\gamma_D : \quad & Y \to Z \\
& u \mapsto \gamma_D u.
\end{aligned}
$$

As usual in EIT, we restore uniqueness of the solution u of the Neumann problem (2) by requiring that the Dirichlet trace $\gamma_D u$ satisfies

$$
\int_{\partial \Omega} \gamma_D u(s) ds = 0.
\tag{4}
$$

Note that to ensure the solvability of the Neumann problem (2) the current j must satisfy the integrability condition, which, in the absence of a source term, reads $\int_{\partial \Omega} j(s) ds = 0$. The associated linear forward operator of the Neumann problem, which maps an input current j to the solution u, is denoted by

$$
\begin{aligned}
F_N^\sigma : \quad & X \to \ Y \\
& j \mapsto \ \ u \ \text{ solves (2).}
\end{aligned}
$$

The linear operator F_D^σ for the Dirichlet problem (3) can be defined analogously. The NtD map can be written as $\gamma_D F_N^\sigma$ and the weak formulation of the Neumann problem (2) becomes

$$
\int_\Omega \sigma \nabla F_N^\sigma(j) \cdot \nabla v dx = \int_{\partial \Omega} j \gamma_D v ds
\tag{5}
$$

for a suitable set of test functions v. The integral on the boundary should be understood in the sense of duality pairing, i.e. $j \in H^{-1/2}(\partial \Omega)$ and $\gamma_D v \in H^{1/2}(\partial \Omega)$ yield $\int_{\partial \Omega} j \gamma_D v ds = \langle j, \gamma_D v \rangle_{H^{-1/2} \times H^{1/2}}$.

As discussed in the Introduction, there are several natural choices for the spaces X, Y and Z. To this end, we introduce

$$
\tilde{H}_\sigma^1(\Omega) = \left\{ u \in L_2(\Omega) \mid \int_\Omega \sigma(x) |\nabla u(x)|^2 dx < \infty, \ \int_{\partial \Omega} \gamma_D u(s) ds = 0 \right\}.
$$

Because of equation (4), the following bilinear form defines a scalar product on this space

$$
\langle u, v \rangle_{\tilde{H}_\sigma^1} = \int_\Omega \sigma \nabla u \cdot \nabla v dx.
$$

3

We use the Dirichlet forward operator F_D^σ as an extension operator and define the following space of functions on the boundary $\partial\Omega$

$$\tilde{H}_\sigma^{1/2}(\partial\Omega) = \left\{ g \in L_2(\partial\Omega) \mid \int_\Omega \sigma(x)|\nabla F_D^\sigma(g)(x)|^2 dx < \infty, \ \int_{\partial\Omega} g(s)ds = 0 \right\}$$

together with its scalar product

$$\langle g, h \rangle_{\tilde{H}_\sigma^{1/2}} = \int_\Omega \sigma(x)\nabla F_D^\sigma(g)(x) \cdot \nabla F_D^\sigma(h)(x)dx.$$

The Dirichlet-to-Neumann (DtN) operator $\sigma\frac{\partial}{\partial n}F_D^\sigma$ is well defined on $\tilde{H}_\sigma^{1/2}(\partial\Omega)$, see [7, 20], and we introduce

$$\tilde{H}_\sigma^{-1/2}(\partial\Omega) = \left\{ f \mid f = \sigma\frac{\partial}{\partial n}F_D^\sigma(g), \ g \in \tilde{H}_\sigma^{1/2}(\partial\Omega) \right\}$$

together with its scalar product

$$\langle f, h \rangle_{\tilde{H}_\sigma^{-1/2}} = \int_\Omega \sigma \nabla F_N^\sigma(f) \cdot \nabla F_N^\sigma(h)dx.$$

We observe, that $f \in \tilde{H}_\sigma^{-1/2}(\partial\Omega)$ is the Neumann trace for $u = F_D^\sigma(g)$. This implies $-\mathrm{div}(\sigma\nabla u) = 0$ and the integrability condition for Neumann problems yields

$$\int_{\partial\Omega} fds = 0 \quad \text{and} \quad \tilde{H}_\sigma^{-1/2}(\partial\Omega) = \left\{ f \in H_\sigma^{-1/2}(\partial\Omega) \mid \int_{\partial\Omega} fds = 0 \right\}.$$

In the following, we will consider the choices $X = \tilde{L}_2(\partial\Omega) = \left\{ f \in L_2(\partial\Omega) \mid \int_{\partial\Omega} f(s)ds = 0 \right\}$ or $X = \tilde{H}_\sigma^{-1/2}(\partial\Omega)$, $Y = \tilde{H}_\sigma^1(\Omega)$ or $Y = L_2(\Omega)$ and $Z = \tilde{H}_\sigma^{1/2}(\partial\Omega)$ or $Z = \tilde{L}_2(\partial\Omega)$. It is well-known that the choice of these function spaces strongly influences analytical and numerical properties of optimal currents, and consequently EIT reconstructions. However, for numerical convenience most authors have studied the $\tilde{L}_2$-case, see, for example [2, Section 7].

3 Functionals for optimal input currents

The design of optimal EIT experiments, i.e. the optimal choice of input currents j, has been the topic of several studies since the pioneering work [13], see also [5, 6, 16]. The basic idea is to construct an input current j that best distinguishes an estimate σ_0 from the unknown physical conductivity σ^*.

In [13], Isaacson compares the NtD maps for σ^* and σ_0 as follows

$$\max_{j, \|j\|_X = 1} \|\gamma_D F_N^{\sigma_0}(j) - \gamma_D F_N^{\sigma^*}(j)\|_Z$$

with $X = Z = \tilde{L}_2(\partial\Omega)$. He then shows that the optimal input current is the maximal eigenfunction (the eigenfunction with the largest eigenvalue in absolute value) of the self-adjoint operator

$$\begin{aligned} A_1 : \tilde{L}_2(\partial\Omega) &\rightarrow \tilde{L}_2(\partial\Omega) \\ j &\mapsto \gamma_D F_N^{\sigma_0}(j) - \gamma_D F_N^{\sigma^*}(j). \end{aligned}$$

We can also use the natural norms in $Z = \tilde{H}_{\sigma_0}^{1/2}(\partial\Omega)$ and $X = \tilde{H}_{\sigma_0}^{-1/2}(\partial\Omega)$. However, these norms depend on σ and we need the following embedding operators ($if = f$)

$$\begin{aligned} i_+ : \quad & \tilde{H}_{\sigma^*}^{1/2}(\partial\Omega) \rightarrow \tilde{H}_{\sigma_0}^{1/2}(\partial\Omega), \\ i_- : \quad & \tilde{H}_{\sigma_0}^{-1/2}(\partial\Omega) \rightarrow \tilde{H}_{\sigma^*}^{-1/2}(\partial\Omega), \end{aligned}$$

where the subscripts $+$ and $-$ refer to the sign of the Sobolev index. We can now define

$$
\begin{aligned}
A_2 : \tilde{H}_{\sigma_0}^{-1/2}(\partial\Omega) &\to \tilde{H}_{\sigma_0}^{1/2}(\partial\Omega) \\
j &\mapsto \gamma_D F_N^{\sigma_0}(j) - i_+ \circ \gamma_D F_N^{\sigma^*} \circ i_- (j).
\end{aligned}
$$

The operator A_2 is no longer self-adjoint and maximizing $\|A_2 j\|_{\tilde{H}_{\sigma_0}^{1/2}}$ requires the computation of a maximal eigenfunction of $A_2^* A_2$.

In [16] another approach for obtaining optimal input currents was introduced by finding

$$
\max_{j,\|j\|_X=1} \| F_N^{\sigma_0}(j) - F_D^{\sigma_0}(\gamma_D F_N^{\sigma^*}(j)) \|_Y .
$$

Incorporating the σ-dependence of the norms involved and taking into account various combinations of function spaces, we define the following operators

$$
\begin{aligned}
A_3 : \tilde{H}_{\sigma_0}^{-1/2}(\partial\Omega) &\to \tilde{H}_{\sigma_0}^1(\Omega) \\
j &\mapsto F_N^{\sigma_0}(j) - F_D^{\sigma_0} \circ i_+ \circ \gamma_D F_N^{\sigma^*} \circ i_- (j), \\
A_4 : \tilde{H}_{\sigma_0}^{-1/2}(\partial\Omega) &\to L_2(\Omega) \\
j &\mapsto F_N^{\sigma_0}(j) - F_D^{\sigma_0} \circ i_+ \circ \gamma_D F_N^{\sigma^*} \circ i_- (j), \\
A_5 : \tilde{L}_2(\partial\Omega) &\to \tilde{H}_{\sigma_0}^1(\Omega) \\
j &\mapsto F_N^{\sigma_0}(j) - F_D^{\sigma_0} \circ i_+ \circ \gamma_D F_N^{\sigma^*}(j), \\
A_6 : \tilde{L}_2(\partial\Omega) &\to L_2(\Omega) \\
j &\mapsto F_N^{\sigma_0}(j) - F_D^{\sigma_0} \circ i_+ \circ \gamma_D F_N^{\sigma^*}(j).
\end{aligned}
$$

The optimal currents based on these functionals are given by the maximal eigenfunctions of $A_k^* A_k$, $k = 3,4,5,6$. In all cases we will take the optimal current as the limit of the iteration

$$
j_{n+1} = \frac{A^* A j_n}{\|A^* A j_n\|},
$$

in the spirit of the power method in linear algebra [11]. To this end, we need to determine $A^* A$ for these combinations of function spaces, and this requires the calculation of the adjoints of the Neumann and the Dirichlet forward operator in different function spaces. This is a classical exercise in PDE-theory for elliptic problems. The restriction to the rather basic equation of EIT makes it even simpler. However, the choice of the somewhat unusual combination of function spaces yield rather different optimal currents as well as different sparse reconstructions.

Remark 3.1 *Another natural functional for obtaining optimal currents is given by*

$$
\max_{j,\|j\|_X=1} \langle j, \gamma_D F_N^{\sigma_0}(j) - \gamma_D F_N^{\sigma^*}(j) \rangle_{\tilde{H}_{\sigma_0}^{-1/2} \times \tilde{H}_{\sigma_0}^{1/2}} .
$$

The choice $X = \tilde{L}_2(\partial\Omega)$ gives

$$
\langle j, \gamma_D F_N^{\sigma_0}(j) - \gamma_D F_N^{\sigma^*}(j) \rangle_{\tilde{H}_{\sigma_0}^{-1/2} \times \tilde{H}_{\sigma_0}^{1/2}} = \langle j, \gamma_D F_N^{\sigma_0}(j) - \gamma_D F_N^{\sigma^*}(j) \rangle_{\tilde{L}_2} ,
$$

which - since the NtD-map is $\tilde{L}_2$-selfadjoint - is equivalent to the case A_1 above.

The choice $X = \tilde{H}_{\sigma_0}^{-1/2}(\partial\Omega)$ is equivalent to cases A_2 and A_3 as we will see in Remark 5.3.

4   Adjoint operators

For a linear continuous operator $B : \mathbb{H}_1 \to \mathbb{H}_2$ between two Hilbert spaces $\mathbb{H}_1$ and $\mathbb{H}_2$, the defining equation for the adjoint operator $B^* : \mathbb{H}_2 \to \mathbb{H}_1$ is given by

$$\langle Bf, g \rangle_{\mathbb{H}_2} = \langle f, B^* g \rangle_{\mathbb{H}_1}.$$

We will determine B^* for the operators (embedding operators i_+ and i_-, NtD operator and Dirichlet and Neumann forward operators F_D^σ and F_N^σ) necessary for constructing optimal currents.

   We will need the following identities.

$$F_D^\sigma = F_N^\sigma \left(\sigma \frac{\partial}{\partial n} F_D^\sigma \right), \tag{6}$$

$$\sigma \frac{\partial}{\partial n} F_D^\sigma \circ \gamma_D F_N^\sigma (f) = f. \tag{7}$$

The second identity states that the DtN map is inverted by the NtD map.

Lemma 4.1 *Let $i : \mathbb{H}_1 \to \mathbb{H}_2$ be the embedding operator. Then the adjoint $i^* : \mathbb{H}_2 \to \mathbb{H}_1$ is given by*

(a) $i^* g = \gamma_D F_N^{\sigma^*} \circ \sigma_0 \frac{\partial}{\partial n} F_D^{\sigma_0}(g)$ *for* $\mathbb{H}_1 = \tilde{H}_{\sigma^*}^{1/2}(\partial\Omega)$ *and* $\mathbb{H}_2 = \tilde{H}_{\sigma_0}^{1/2}(\partial\Omega)$,

(b) $i^* g = \sigma_0 \frac{\partial}{\partial n} F_D^{\sigma_0} \circ \gamma_D F_N^{\sigma^*}(g)$ *for* $\mathbb{H}_1 = \tilde{H}_{\sigma_0}^{-1/2}(\partial\Omega)$ *and* $\mathbb{H}_2 = \tilde{H}_{\sigma^*}^{-1/2}(\partial\Omega)$.

Proof. (a), here $i = i_+$ and by utilizing $i_+ f = f$, the definition of the norm in $\tilde{H}_{\sigma_0}^{1/2}(\partial\Omega)$, the weak formulation (5) of the Neumann problem and identity (6), we deduce that

$$\langle i_+ f, g \rangle_{\tilde{H}_{\sigma_0}^{1/2}} = \int_\Omega \sigma_0(x) \nabla F_D^{\sigma_0}(f)(x) \cdot \nabla F_D^{\sigma_0}(g)(x) dx$$

$$= \int_\Omega \sigma_0(x) \nabla F_D^{\sigma_0}(f)(x) \cdot \nabla F_N^{\sigma_0} \left(\sigma_0 \frac{\partial}{\partial n} F_D^{\sigma_0}(g) \right)(x) dx$$

$$= \int_{\partial\Omega} f(s) \sigma_0(s) \frac{\partial}{\partial n} F_D^{\sigma_0}(g)(s) ds.$$

Similarly

$$\langle f, i_+^* g \rangle_{\tilde{H}_{\sigma^*}^{1/2}} = \int_\Omega \sigma^*(x) \nabla F_D^{\sigma^*}(f)(x) \cdot \nabla F_D^\sigma(i_+^* g)(x) dx$$

$$= \int_{\partial\Omega} f(s) \sigma^*(s) \frac{\partial}{\partial n} F_D^{\sigma^*}(i_+^* g)(s) ds.$$

Now comparing the scalar products and using identity (7) yields the first assertion.

   (b) Here $i = i_-$. Appealing again to the weak formulation (5) of the Neumann problem and the definition of the norm in $\tilde{H}_{\sigma_0}^{-1/2}(\partial\Omega)$ yields

$$\langle i_- f, g \rangle_{\tilde{H}_{\sigma^*}^{-1/2}} = \int_\Omega \sigma^*(x) \nabla F_N^{\sigma^*}(f)(x) \cdot \nabla F_N^{\sigma^*}(g)(x) dx$$

$$= \int_{\partial\Omega} f(s) \gamma_D F_N^{\sigma^*}(g)(s) ds,$$

$$\langle f, i_-^* g \rangle_{\tilde{H}_{\sigma_0}^{-1/2}} = \int_\Omega \sigma_0(x) \nabla F_N^{\sigma_0}(f)(x) \cdot \nabla F_N^{\sigma_0}(i_-^* g)(x) dx$$

$$= \int_{\partial\Omega} f(s) \gamma_D F_N^{\sigma_0}(i_-^* g)(s) ds.$$

Comparing the scalar products and using equation (7) gives the second assertion. ∎

Next we consider the NtD operator $B := \gamma_D F_N^\sigma : X \to Z$ for different combinations of function spaces. It is well-known that $B : \tilde{L}_2(\partial\Omega) \to \tilde{L}_2(\partial\Omega)$ is self-adjoint, i.e. $B^* = \gamma_D F_N^\sigma$, and similarly the adjoint of $B : \tilde{H}_\sigma^{-1/2}(\partial\Omega) \to \tilde{H}_\sigma^{1/2}(\partial\Omega)$ is given by the DtN map, i.e. $B^* = \sigma\frac{\partial}{\partial n} F_D^\sigma$, see [2]. The next result gives the adjoint for $B : \tilde{L}_2(\partial\Omega) \to \tilde{H}_\sigma^{1/2}(\partial\Omega)$.

Lemma 4.2 *The adjoint of the NtD map $B = \gamma_D F_N^\sigma : \tilde{L}_2(\partial\Omega) \to \tilde{H}_\sigma^{1/2}(\partial\Omega)$ is the embedding operator*

$$
\begin{aligned}
B^* : \tilde{H}_\sigma^{1/2}(\partial\Omega) &\to \tilde{L}_2(\partial\Omega) \\
f &\mapsto B^* f = f.
\end{aligned}
$$

Proof. The defining equation for the adjoint operator is

$$
\langle Bg, f \rangle_{\tilde{H}_\sigma^{1/2}} = \langle g, B^* f \rangle_{\tilde{L}_2} = \int_{\partial\Omega} g(s)(B^* f)(s)ds.
$$

The identity $F_D^\sigma(Bg) = F_D^\sigma(\gamma_D F_N^\sigma(g)) = F_N^\sigma(g)$ and the definition of the norm in $\tilde{H}_\sigma^{1/2}(\partial\Omega)$ in conjunction with the weak formulation of the Neumann problem yield

$$
\begin{aligned}
\langle Bg, f \rangle_{\tilde{H}_\sigma^{1/2}} &= \int_\Omega \sigma \nabla F_D^\sigma(Bg) \cdot \nabla F_D^\sigma(f) dx \\
&= \int_\Omega \sigma \nabla F_N^\sigma(g) \cdot \nabla F_D^\sigma(f) dx = \int_{\partial\Omega} g(s)f(s)ds.
\end{aligned}
$$

Comparing these scalar products implies $B^* f = f$. $\blacksquare$

The next lemma summarizes the adjoints for the Neumann forward operator F_N^σ. Observing the integrability condition, the natural choices for the function spaces X and Y for Neumann forward operators are $X = \tilde{L}_2(\partial\Omega)$ or $X = \tilde{H}_\sigma^{-1/2}(\partial\Omega)$ and $Y = L_2(\Omega)$ or $Y = \tilde{H}_\sigma^1(\Omega)$.

Lemma 4.3 *Let $B = F_N^\sigma : X \to Y$ be the Neumann forward operator. For any $u \in Y$ let z be the solution of the inhomogeneous Neumann problem with source term u and constant boundary data $c = -\int_\Omega u(x)dx/|\partial\Omega|$. Then the adjoint $B^* : Y \to X$ is given by*

(a) $B^* u = \sigma\frac{\partial}{\partial n} F_D^\sigma(\gamma_D u)$ *for $X = \tilde{H}_\sigma^{-1/2}(\partial\Omega)$ and $Y = \tilde{H}_\sigma^1(\Omega)$,*

(b) $B^* u = \sigma\frac{\partial}{\partial n} F_D^\sigma(\gamma_D z)$ *for $X = \tilde{H}_\sigma^{-1/2}(\partial\Omega)$ and $Y = L_2(\Omega)$,*

(c) $B^* u = \gamma_D z$ *for $X = \tilde{L}_2(\partial\Omega)$ and $Y = L_2(\Omega)$,*

(d) $B^* u = \gamma_D u$ *for $X = \tilde{L}_2(\partial\Omega)$ and $\tilde{H}_\sigma^1(\Omega)$.*

Proof. (a). The weak formulation of the Neumann problem for $F_N^\sigma(f)$ stated in (5) gives

$$
\begin{aligned}
\langle f, B^* u \rangle_X &= \int_\Omega \sigma(x)\nabla F_N^\sigma(f)(x) \cdot \nabla F_N^\sigma(B^* u)(x)dx \\
&= \int_{\partial\Omega} f(s)\gamma_D F_N^\sigma(B^* u)(s)ds.
\end{aligned}
$$

On the other hand, we have

$$
\langle Bf, u \rangle_Y = \int_\Omega \sigma(x)\nabla F_N^\sigma(f)(x) \cdot \nabla u(x)dx = \int_{\partial\Omega} f(s)\gamma_D u(s)ds.
$$

Comparing these two identities yields $\gamma_D F_N^\sigma(B^*u) = \gamma_D u(s)$ and the desired identity follows using (7).

It remains to verify the integrability condition of B^*u, i.e. $B^*u \in \tilde{H}_\sigma^{-1/2}(\partial\Omega)$. Let $w = F_D^\sigma(\gamma_D u)$, then we have $-\mathrm{div}(\sigma\nabla w) = 0$. The assertion follows from the integrability condition for the Neumann problem with vanishing sources, i.e.

$$0 = \int_{\partial\Omega} \sigma \frac{\partial}{\partial n} w(s)ds = \int_{\partial\Omega} B^*u(s)ds.$$

(b). From the definition of the scalar product in X and the weak formulation of the Neumann problem for $F_N^\sigma(f)$, we obtain

$$\langle f, B^*u \rangle_X = \int_\Omega \sigma(x)\nabla F_N^\sigma(f)(x) \cdot \nabla F_N^\sigma(B^*u)(x)dx = \langle f, \gamma_D F_N^\sigma(B^*u)\rangle_{H_\sigma^{-1/2} \times H_\sigma^{1/2}}.$$

Let z be the solution of the inhomogeneous Neumann problem with source term $u \in L_2(\Omega)$ and constant Neumann boundary data $c = -\int_\Omega u dx/|\partial\Omega|$. The choice of c ensures the integrability condition. Utilizing the weak formulation for z with test function Bf we obtain

$$
\begin{aligned}
\langle z, Bf \rangle_{\tilde{H}_\sigma^1} &= \langle u, Bf \rangle_{(\tilde{H}_\sigma^1)' \times \tilde{H}_\sigma^1} + \langle c, \gamma_D Bf \rangle_{H_\sigma^{-1/2} \times H_\sigma^{1/2}} \\
&= \langle u, Bf \rangle_{L_2} + \int_{\partial\Omega} c\, \gamma_D Bf ds = \langle u, Bf \rangle_{L_2},
\end{aligned}
$$

where we have used the normalization for the Neumann forward solver B, see equation (4). Utilizing the weak formulation of the Neumann problem for $Bf = F_N^\sigma(f)$ with test function z yields

$$\langle z, Bf \rangle_{\tilde{H}_\sigma^1} = \langle \gamma_D z, f \rangle_{H_\sigma^{-1/2} \times H_\sigma^{1/2}}.$$

By combining the preceding three expressions we obtain

$$\gamma_D F_N^\sigma(B^*u) = \gamma_D z,$$

which together with equation (7) gives the desired result. It remains to check $B^*u \in \tilde{H}_\sigma^{-1/2}(\partial\Omega)$. Note that since $w = F_D^\sigma(\gamma_D z)$ satisfies $-\mathrm{div}(\sigma\nabla w) = 0$ the Neumann integrability condition implies $\int_{\partial\Omega} \sigma \frac{\partial}{\partial n} w ds = 0$ and hence $B^*u \in \tilde{H}_\sigma^{-1/2}(\partial\Omega)$.

Similarly, we obtain that for Case (c), i.e. $B : \tilde{L}_2(\partial\Omega) \to L_2(\Omega)$, $B^*u = \gamma_D z$, where z is the solution of the inhomogeneous Neumann problem with source term u and constant boundary value $c = -\int_\Omega u(x)dx/|\partial\Omega|$. Equation (4) implies $\int_{\partial\Omega} \gamma_D z(s)ds = 0$, i.e. $B^*u \in \tilde{L}_2(\partial\Omega)$.

For Case (d), i.e. $B : \tilde{L}_2(\partial\Omega) \to \tilde{H}^1(\Omega)$, we can deduce analogously that $B^*u = \gamma_D u$. ∎

Remark 4.4 *We can simplify the expression for Case (a) if u is the solution of a homogeneous Dirichlet problem. In this case we obtain*

$$B^*u = \sigma \frac{\partial}{\partial n} F_D^\sigma(\gamma_D u) = \sigma \frac{\partial}{\partial n} u.$$

Finally, we consider the adjoint for the Dirichlet forward operator $B = F_D^\sigma : X \to Y$.

Lemma 4.5 *Let $B = F_D^\sigma : X \to Y$ be the Dirichlet forward operator. For any $u \in Y$ let z be the solution of the inhomogeneous Neumann problem with source term u and constant boundary data $c = -\int_\Omega u(x)dx/|\partial\Omega|$. Then the adjoint $B^* : Y \to X$ is given by*

(a) $B^*u = \gamma_{D} u$ for $X = \tilde{H}_\sigma^{1/2}(\partial\Omega)$ and $Y = \tilde{H}_\sigma^1(\Omega)$,

(b) $B^*u = \gamma_{D} z$ for $X = \tilde{H}_\sigma^{1/2}(\partial\Omega)$ and $Y = L_2(\Omega)$.

Proof. (a), using identity (6) and Lemma 4.3, we obtain

$$
\begin{aligned}
B^*u &= (F_N^\sigma \circ \sigma \tfrac{\partial}{\partial n} F_D^\sigma)^*(u) \\
&= \left(\sigma \tfrac{\partial}{\partial n} F_D^\sigma\right)^* \circ (F_N^\sigma)^*(u) \\
&= \gamma_{D} F_N^\sigma \circ \sigma \tfrac{\partial}{\partial n} F_D^\sigma (\gamma_{D} u) = \gamma_{D} u.
\end{aligned}
$$

(b), the Neumann forward operator F_N^σ is now a mapping from $\tilde{H}_\sigma^{-1/2}(\partial\Omega)$ to $L_2(\Omega)$. Using identity (6) and Lemma 4.3, we deduce

$$
\begin{aligned}
B^*u &= (F_N^\sigma \circ \sigma \tfrac{\partial}{\partial n} F_D^\sigma)^*(u) \\
&= \left(\sigma \tfrac{\partial}{\partial n} F_D^\sigma\right)^* \circ (F_N^\sigma)^*(u) \\
&= \gamma_{D} F_N^\sigma \circ \sigma \tfrac{\partial}{\partial n} F_D^\sigma (\gamma_{D} z) = \gamma_{D} z,
\end{aligned}
$$

where z is the solution of the inhomogeneous Neumann problem with source term u and constant Neumann boundary data $c = -\int_\Omega u\,dx/|\partial\Omega|$. ∎

5 Optimal input currents

As motivated in Section 1, we search for an input current j that distinguishes the physical model σ^* from an estimate σ_0. We compute the optimal input current j^* by the power method

$$
j_{n+1} = \frac{A^* A j_n}{\|A^* A j_n\|},
$$

which converges to an optimal current for general j_0. In Section 3 we introduced several choices for A, which resulted from different discrepancy functionals and choices of function spaces. These approaches will lead to a variety of 'optimal' input currents. The analytical differences between these 'optimal' currents can be expressed by comparing the NtD and DtN operators for σ^* and σ_0. More precisely, we introduce

$$
E = \sigma_0 \tfrac{\partial}{\partial n} F_D^{\sigma_0} \circ \gamma_{D} F_N^{\sigma^*} \quad \text{and} \quad \tilde{E} = \gamma_{D} F_N^{\sigma^*} \circ \sigma_0 \tfrac{\partial}{\partial n} F_D^{\sigma_0}.
$$

Both operators reduce to the identity operator if $\sigma_0 = \sigma^*$. In the following theorem we give the main analytical result of this paper.

Theorem 5.1 *Let E, and $\tilde{E}$ be defined as above. Let $u = F_N^{\sigma_0}(1-E)j$ and let z be the solution of the inhomogeneous Neumann problem with conductivity σ_0, source term u and constant boundary value $c = -\int_\Omega u\,dx/|\partial\Omega|$. Then*

(a) $A_1^* : \tilde{L}_2(\partial\Omega) \to \tilde{L}_2(\partial\Omega)$ and $A_1^* = A_1 = \gamma_{D} F_N^{\sigma_0} \circ (1-E)$,

(b) $A_2^* A_2 = A_3^* A_3 : \tilde{H}_{\sigma_0}^{-1/2}(\partial\Omega) \to \tilde{H}_{\sigma_0}^{-1/2}(\partial\Omega)$ and $A_2^* A_2 = A_3^* A_3 = (1-E)^2$,

(c) $A_4^* A_4 : \tilde{H}_{\sigma_0}^{-1/2}(\partial\Omega) \to \tilde{H}_{\sigma_0}^{-1/2}(\partial\Omega)$ and $A_4^* A_4 f = \sigma_0 \tfrac{\partial}{\partial n} F_D^{\sigma_0} \circ (1-\tilde{E}) \circ \gamma_{D} z$,

(d) $A_5^* A_5 : \tilde{L}_2(\partial\Omega) \to \tilde{L}_2(\partial\Omega)$ and $A_5^* A_5 = \gamma_{D} F_N^{\sigma_0}(1-E)^2$,

(e) $A_6^* A_6 : \tilde{L}_2(\partial\Omega) \to \tilde{L}_2(\partial\Omega)$ and $A_6^* A_6 f = (1-\tilde{E}) \circ \gamma_{D} z$.

<div align="center">9</div>

Proof. Case (a). The L_2-norm does not depend on σ which is the only case not requiring embedding operators. The NtD operator is self-adjoint as a mapping $\tilde{L}_2(\partial\Omega) \to \tilde{L}_2(\partial\Omega)$ and

$$A_1^* = (\gamma_D F_N^{\sigma_0})^* - (\gamma_D F_N^{\sigma^*})^* = A_1.$$

Case (b). By the definition of the norm in $\tilde{H}_{\sigma_0}^{1/2}(\partial\Omega)$, we have $\|A_2 j\|_{\tilde{H}_{\sigma_0}^{1/2}} = \|F_D^{\sigma_0}(A_2 j)\|_{\tilde{H}_{\sigma_0}^1}$, and moreover, we observe

$$
\begin{aligned}
F_D^{\sigma_0}(A_2 j) &= F_D^{\sigma_0}(\gamma_D F_N^{\sigma_0}(j) - i_+\gamma_D F_N^{\sigma^*}(i_- j))) \\
&= F_N^{\sigma_0}(j) - F_D^{\sigma_0}(i_+\gamma_D F_N^{\sigma^*}(i_- j)) = A_3 j,
\end{aligned}
$$

i.e. $\|A_2 j\|_{\tilde{H}_{\sigma_0}^{1/2}} = \|A_3 j\|_{\tilde{H}_{\sigma_0}^1}$ and the iterations for $A_2^* A_2$ and $A_3^* A_3$ are the same. Therefore, it suffices to consider only A_3. To this end, we split A_3 as follows $A_3 j = Cj - Dj$ with $Cj = F_N^{\sigma_0}(j)$ and $Dj = F_D^{\sigma_0}(i_+\gamma_D F_N^{\sigma^*}(i_- j))$, respectively. By Lemma 4.3 we have

$$C^* u = \sigma_0 \frac{\partial}{\partial n} F_D^{\sigma_0}(\gamma_D u),$$

and Lemmas 4.1-4.3 and Lemma 4.5 imply

$$
\begin{aligned}
D^* u &= (i_-)^* \circ (\gamma_D F_N^{\sigma^*})^* \circ (i_+)^* \circ (F_D^{\sigma_0})^* u \\
&= \sigma_0 \frac{\partial}{\partial n} F_D^{\sigma_0} \circ \gamma_D F_N^{\sigma^*} \circ \sigma^* \frac{\partial}{\partial n} F_D^{\sigma^*} \circ \gamma_D F_N^{\sigma^*} \circ \sigma_0 \frac{\partial}{\partial n} F_D^{\sigma_0} \circ \gamma_D u \\
&= \sigma_0 \frac{\partial}{\partial n} F_D^{\sigma_0} \circ \gamma_D F_N^{\sigma^*} \circ \sigma_0 \frac{\partial}{\partial n} F_D^{\sigma_0} \circ \gamma_D u.
\end{aligned}
$$

Combining these adjoint operators and recalling the definition of the operator E gives

$$
\begin{aligned}
A_3^* A_3 j &= (C^*C - C^*D - D^*C + D^*D)j \\
&= j - \sigma_0 \frac{\partial}{\partial n} F_D^{\sigma_0}(\gamma_D F_N^{\sigma^*}(j)) - \sigma_0 \frac{\partial}{\partial n} F_D^{\sigma_0} \circ \gamma_D F_N^{\sigma^*} \circ \sigma_0 \frac{\partial}{\partial n} F_D^{\sigma_0} \circ \gamma_D \circ F_N^{\sigma_0}(j) \\
&\quad + \sigma_0 \frac{\partial}{\partial n} F_D^{\sigma_0} \circ \gamma_D F_N^{\sigma^*} \circ \sigma_0 \frac{\partial}{\partial n} F_D^{\sigma_0} \circ \gamma_D F_D^{\sigma_0}(\gamma_D F_N^{\sigma^*}(j)) \\
&= j - 2\sigma_0 \frac{\partial}{\partial n} F_D^{\sigma_0}(\gamma_D F_N^{\sigma^*}(j)) + \sigma_0 \frac{\partial}{\partial n} F_D^{\sigma_0} \circ \gamma_D F_N^{\sigma^*} \circ \sigma_0 \frac{\partial}{\partial n} F_D^{\sigma_0} \circ \gamma_D (F_N^{\sigma^*}(j)) \\
&= (1 - E)^2 j.
\end{aligned}
$$

Case (c). Again we split the operator A_4 as $A_4 j = Cj - Dj$ with C and D as in Case (b). As opposed to Case (b), $F_N^{\sigma_0}$, respectively $F_D^{\sigma_0}$, is a mapping $\tilde{H}_{\sigma_0}^{-1/2}(\partial\Omega) \to L_2(\Omega)$, respectively $\tilde{H}_{\sigma_0}^{1/2}(\partial\Omega) \to L_2(\Omega)$. With the help of the results in Section 4 and taking into account the definitions of u and z, we obtain

$$C^* u = \sigma_0 \frac{\partial}{\partial n} F_D^{\sigma_0}(\gamma_D z),$$

and similarly we have

$$
\begin{aligned}
D^* u &= (i_-)^* \circ (\gamma_D F_N^{\sigma^*})^* \circ (i_+)^* \circ (F_D^{\sigma_0})^* u \\
&= \sigma_0 \frac{\partial}{\partial n} F_D^{\sigma_0} \circ \gamma_D F_N^{\sigma^*} \circ \sigma_0 \frac{\partial}{\partial n} F_D^{\sigma_0} \circ \gamma_D z.
\end{aligned}
$$

Combining these adjoint operators we obtain $C^*(C - D) = \sigma_0 \frac{\partial}{\partial n} F_D^{\sigma_0}(\gamma_D z)$ where z is the weak solution of $-div\sigma_0\nabla = F_N^{\sigma_0}(1 - E)j$ with constant Neumann data. Similarly, we compute $D^*(C - D)$ and the definition of $\tilde{E}$ gives the third assertion.

Case (d). We appeal again to the splitting $A_5 j = Cj - Dj$ with $Cj = F_N^{\sigma_0}(j)$ and $Dj = F_D^{\sigma_0}(i_+ \gamma_D F_N^{\sigma^*}(j))$. Now $F_N^{\sigma_0}$, respectively $\gamma_D F_N^{\sigma^*}$, acts as a mapping $\tilde{L}_2(\partial\Omega) \to \tilde{H}_{\sigma_0}^1(\Omega)$, respectively $\tilde{L}_2(\partial\Omega) \to \tilde{H}_{\sigma^*}^{1/2}(\partial\Omega)$. Using the results in Section 4, we deduce that

$$C^* u = \gamma_D u$$

and

$$
\begin{aligned}
D^* u &= (\gamma_D F_N^{\sigma^*})^* \circ (i_+)^* \circ (F_D^{\sigma_0})^* u \\
&= \gamma_D F_N^{\sigma^*} \circ \sigma_0 \frac{\partial}{\partial n} F_D^{\sigma_0} \circ \gamma_D u.
\end{aligned}
$$

The fourth assertion follows directly from these two adjoint operators and identity (7).

Case (e). We once again appeal to the splitting $A_6 j = Cj - Dj$ with C and D as in Case (d). Recall that $F_N^{\sigma_0}$, respectively $F_D^{\sigma_0}$, is a mapping $\tilde{L}_2(\partial\Omega) \to L_2(\Omega)$, respectively $\tilde{H}_{\sigma_0}^{1/2}(\partial\Omega) \to L_2(\Omega)$. With the definitions of u and z, we obtain

$$C^* u = \gamma_D z$$

and

$$
\begin{aligned}
D^* u &= (\gamma_D F_N^{\sigma^*})^* \circ (i_+)^* \circ (F_D^{\sigma_0})^* u \\
&= \gamma_D F_N^{\sigma^*} \circ \sigma_0 \frac{\partial}{\partial n} F_D^{\sigma_0} \circ \gamma_D z.
\end{aligned}
$$

The last assertion follows easily from these adjoint operators. ∎

Remark 5.2 *(1) The description of $A^* A$ has been chosen for the convenience of analytic comparison. For numerical implementations it is more convenient to use e.g. $\gamma_D F_N^{\sigma_0} \circ (1 - E) = \gamma_D F_N^{\sigma_0} - \gamma_D F_N^{\sigma^*}$.*

(2) The power method for case (b) can be simplified to $j_{n+1} = \frac{A_1 j_n}{\|A_1 j_n\|}$, which is the classical case treated already in [13].

Remark 5.3 *We conclude this section with a remark on the functional introduced in Remark 3.1. For $X = \tilde{H}_{\sigma_0}^{-1/2}(\partial\Omega)$ this can be simplified by using the Riesz map $\tilde{H}_{\sigma_0}^{-1/2}(\partial\Omega) \to \tilde{H}_{\sigma_0}^{1/2}(\partial\Omega)$, which is the NtD-map $\gamma_D F_N^{\sigma_0}$. We apply the adjoint of the Riesz map and obtain:*

$$\langle j, \gamma_D F_N^{\sigma_0}(j) - \gamma_D F_N^{\sigma^*}(j)\rangle_{\tilde{H}_{\sigma_0}^{-1/2} \times \tilde{H}_{\sigma_0}^{1/2}} = \langle j, (1-E)j\rangle_{\tilde{H}_{\sigma_0}^{-1/2}}.$$

The operator $(1 - E)$ is selfadjoint as a mapping $\tilde{H}_{\sigma_0}^{-1/2}(\partial\Omega) \to \tilde{H}_{\sigma_0}^{-1/2}(\partial\Omega)$. In addition $(1 - E)$ is a postive operator in a neigborhood of σ^*, hence, the functional of Remark 3.1 yields the same optimal currents as A_2 above.

6 Numerical experiments

This section consists of two parts. In the first, we present some numerical results on the construction of optimal currents by maximizing the discrepancy functionals introduced in Section 3. We will always implement the power method which requires us to compute iterations with $A_k^* A_k, k = 1, .., 6$, see Section 5. The second part is devoted to a comparison of these different optimal currents in terms of their usefulness for solving the inverse EIT problem. As a full reconstruction scheme is beyond the scope of this article, we will restrict ourselves to a numerical implementation of a simplified sparsity scheme and compare the resulting reconstructions.
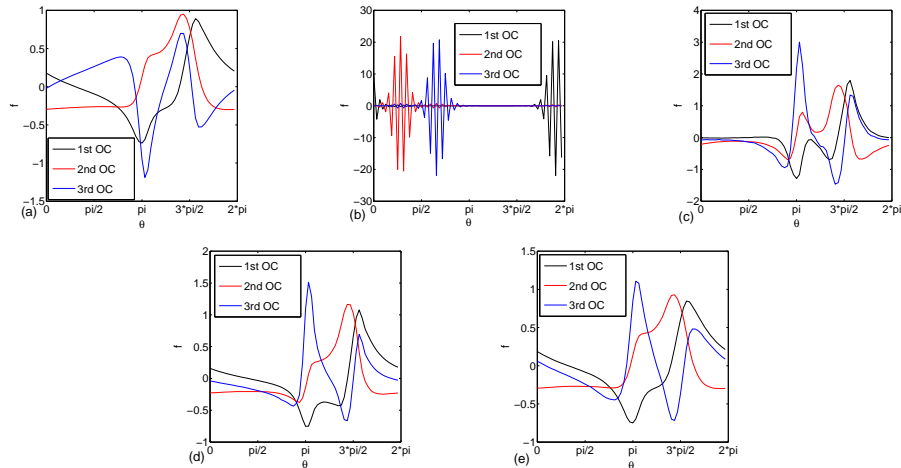
Figure 1: The first three optimal currents for (a) Case 1, (b) Cases 2 and 3, (c) Case 4, (d) Case 5, and (e) Case 6.

6.1 Numerical computation of optimal EIT currents

As in other numerical studies we use a test problem which aims at detecting small inclusions within a homogeneous background. For a survey on this topic see, for example, [2, 4]. The domain Ω is taken to be a unit disk and the background conductivity is set to $\sigma_0 = 1$ which is also always our choice of the initial estimate σ_0.

We have tested the computation of the optimal currents with a single inclusion at different locations as well as with multiple inclusions of varying conductivity. The influence of the function space settings on the resulting optimal current is well illustrated in the following test scheme: we choose two circular inclusions, one centred at $(0, -0.6)$ with a radius 0.3 and another centred at $(-0.7, 0)$ with a radius 0.2. Both inhomogeneities have a conductivity 6.

The Dirichlet and Neumann problems were discretized using piecewise linear finite elements with 1032 finite elements. The initial guesses j_0 for optimal currents (OC) are generated randomly, and we have always computed $n = 1000$ iterations of $j_{n+1} = A^*Aj_n/\|A^*Aj_n\|$. With the exception of Case 3, the convergence of the power method is rather fast and typically $n = 20$ or fewer iterations are sufficient to obtain a good approximation of the optima current. In addition, we have computed the eigenfunctions of A^*A corresponding to the second and third largest eigenvalues by subsequent orthogonalization using a Gram-Schmidt procedure. The iteration applies to the orthogonal basis in the spirit of classical QR algorithm [11]. The converged profile of the first three optimal currents are shown in Figure 1, where θ refers to the angular coordinate on the boundary $\partial\Omega$.

As expected the optimal currents are localized at those parts of the boundary which are close to the inclusions. The optimal current of Case 1 is similar to Cases 5 and 6. However, Case 4 has the sharpest localization, i.e. the optimal current decays quickly to zero away from the inclusions and it allows a clean discrimination between the two inclusions. Nevertheless, all these four cases can locate correctly the position of the inhomogeneities.

Surprisingly, Cases 2 and 3 fail to produce any physically interesting optimal currents. A closer examination of the iteration of Case 3 reveals that the final step in each iteration is the computation of Neumann boundary data. Hence the iterates are elements of $H_{\sigma_0}^{-1/2}(\partial\Omega)$ which is a set of measures rather than a set of functions. The oscillations observed in the optimal currents reflect the mesh size of the discretization. The oscillations increase for finer discretizations but

12

Table 1: The error of the reconstruction for Test 1 with 1% noise.

Case	1	2,3	4	5	6
1st OC	1.692	-	1.573	1.619	1.664
2nd OC	1.439	-	1.437	1.444	1.421

the envelope is stable. Nevertheless, the optimal currents computed for Case 3 seem nonphysical and the locations of the optimal current are completely misleading.

The iteration of Case 4 also involves the computation of Neumann boundary data as a final step. However, this iteration also involves an intermediate solution of a Neumann problem, which yields elements in $\tilde{H}^1_{\sigma_0}(\Omega)$. This can be regarded as an intermediate smoothing and leads to a stabilization of the iteration procedure.

The eigenfunctions corresponding to the second and third largest eigenvalues exhibit additional features. Those for Cases 1, 5 and 6 are quite similar, and those for Case 4 remain more narrowly supported around the positions of the inhomogeneities. Intuitively we might expect that this would lead to better reconstructions. The difference between these two categories appears to originate from the different norms for the fluxes j: the former uses $\tilde{L}_2(\partial\Omega)$, whereas the latter uses $\tilde{H}^{-1/2}_{\sigma_0}(\partial\Omega)$.

6.2 Evaluation of the different optimal currents

Each of the optimal currents discussed in this paper is derived from maximizing a specific functional. How can we decide which of these different optimal currents is the best? For this we need an additional criterion which is independent of the functionals. We have chosen a criterion which allows us to illustrate the potential of these optimal currents for reconstructing local inhomogeneities. Since such a conductivity distribution exhibits a sparse structure we use a sparse reconstruction scheme. We expect that this will not only allow us to locate the inclusions but will, in addition, give qualitatively acceptable reconstruction values.

Our sparse reconstruction algorithm is based on the iterated soft shrinkage scheme S_λ for non-linear operator equations developed in [21, 1, 3]. This scheme requires us to compute the derivative with respect to σ of the following functional

$$J(\sigma) = \int_\Omega \sigma |\nabla(F^\sigma_N(j) - F^\sigma_D(\varphi^\delta))|^2 dx$$

where φ^δ is the measured potential data of an EIT experiment with optimal current j. The iterated soft shrinkage scheme for updating σ proceeds now by computing the usual gradient descent step followed by a soft shrinkage step

$$\sigma_1 = S_{s\alpha}\left(\sigma_0 - sJ'(\sigma_0)\right),$$

where s is the step size determined by Armijo's rule and α is the threshold parameter. The shrinkage operator S_λ promotes the sparse structure of the reconstructions. It can be shown that for the functional $J(\sigma)$, the gradient $J'(\sigma_0)$ is given by

$$J'(\sigma_0) = |\nabla F^{\sigma_0}_D(\varphi^\delta)|^2 - |\nabla F^{\sigma_0}_N(j)|^2.$$

In addition we have incorporated a smoothing of $J'(\sigma_0)$ using an inverse Laplacian in order to stabilize the iteration.

The sparsity-promoting reconstructions using the optimal currents are shown in Figure 2, where the results for Cases 2 and 3 are not presented due to their poor quality. The threshold
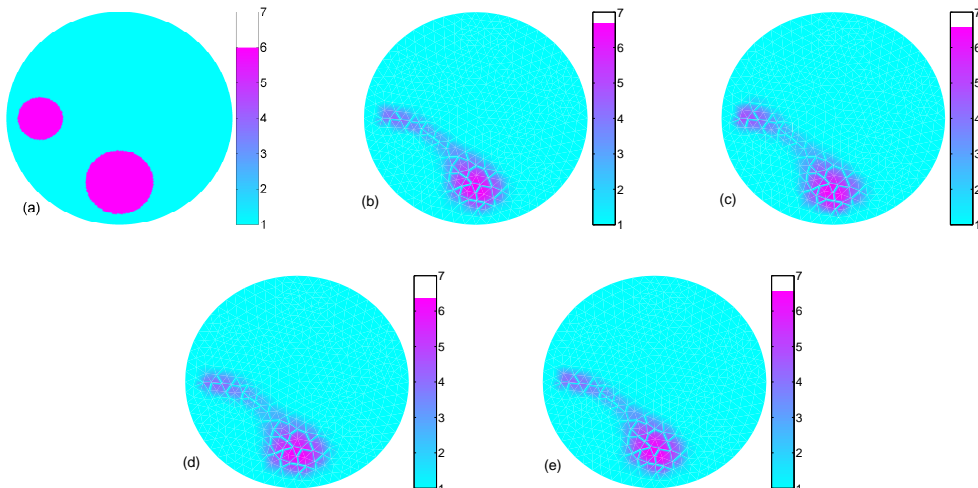
13

Figure 2: (a) exact σ^* and numerical reconstruction with the first optimal current of (b) Case 1, (c) Case (4), (d) Case 5 and (e) Case 6.

Table 2: The error of the reconstruction for Test 2 with 1% noise.

Case	1	2,3	4	5	6
1st OC	1.575	-	1.575	1.723	1.578
2nd OC	1.609	-	1.615	1.658	1.656

parameter assumes the role of the regularization parameter and its value was taken to be $\alpha = 5 \times 10^{-4}$. For the results presented, 1% relative noise was added to the exact data which were generated using a finer finite element mesh with 4128 finite elements. The algorithm was stopped after 400 iterations.

The reconstructions accurately determine the location of inhomogeneities for all remaining cases (Cases 1, 4, 5 and 6), and the results are practically identical. Note that the smaller inclusion is less well resolved compared to the larger one. Nonetheless, the estimate remains acceptable taking into account the fact that we have used only one optimal current. Most interestingly, the magnitude of the larger inclusion was correctly retrieved and this contrasts sharply with most existing methods that typically determine only the location with reasonable precision. To measure the accuracy of the reconstructions, we compute the error $\|\sigma^* - \sigma\|_{L_2}$. The errors for these reconstructions are shown in Table 1. The errors are largely comparable with each other, with that for Case 4 being slightly smaller.

We also perform the reconstruction with the eigenfunctions for the second largest eigenvalues, which seem to be localized on the boundary close to the smaller inclusion. The results are shown in Figure 3 and we observe that the numerical results are comparable with those using the optimal currents. An interesting observation is that the location of the smaller inclusion is more accurately and sharply resolved compared to those in Figure 2, and consequently, the accuracy is improved slightly, see Table 1. This indicates that this eigenfunction contains more information about the smaller inclusion, than the first one.

To further evaluate these optimal currents, we consider a more challenging test: the inclusion has again conductivity 6 but it is now centered at $(0, -0.1)$ with radius 0.3. Again the inhomogeneity has conductivity 6. For all cases, the threshold parameter was set to 2×10^{-3}, and the algorithm was stopped after 1000 iterations. The reconstruction results using the optimal
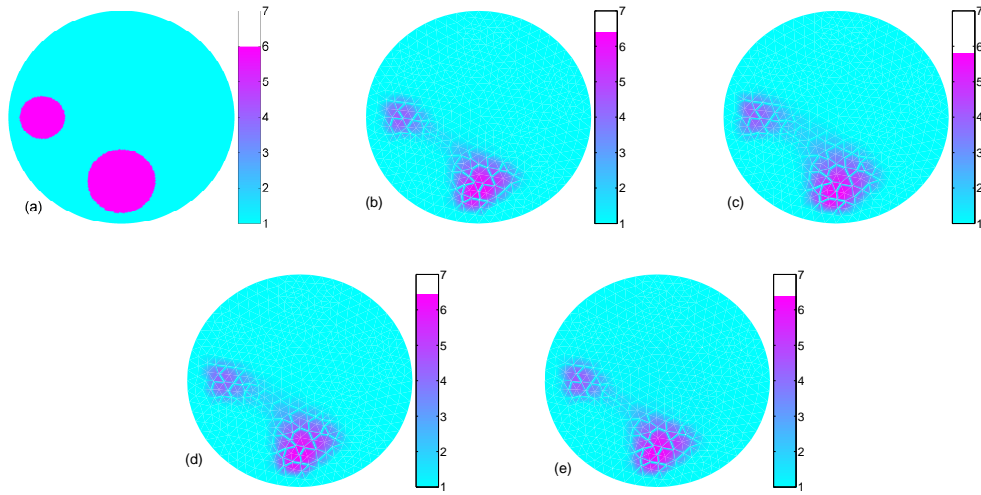
14

Figure 3: (a) exact σ^* and numerical reconstruction with the second optimal current of (b) Case 1, (c) Case (4), (d) Case 5 and (e) Case 6.
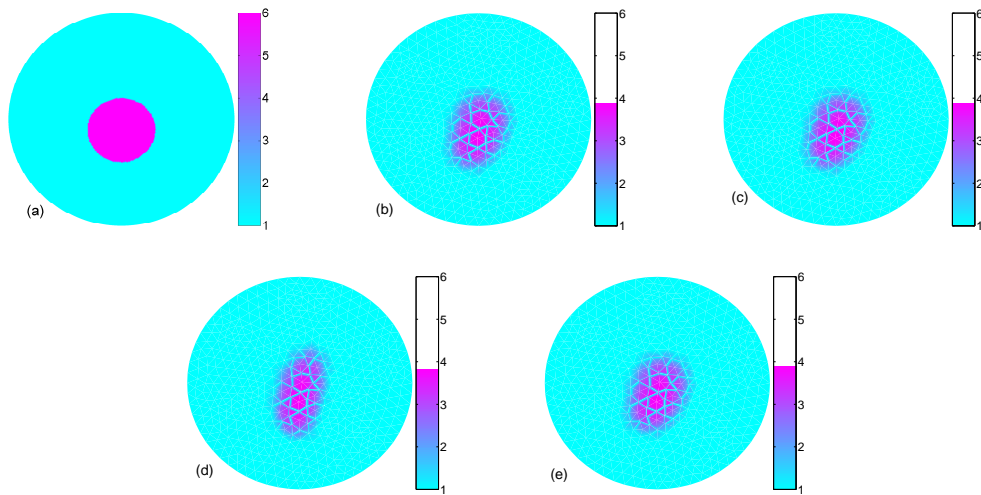

Figure 4: (a) exact σ^* and numerical reconstruction with the first optimal current of (b) Case 1, (c) Case 4, (d) Case 5 and (e) Case 6.

currents are shown in Figure 4. Since the inclusion is located far away from the boundary, a single optimal current does not contain enough information for accurately reconstructing the conductivity. In particular, for all the cases, the retrieved magnitude is significantly smaller than the exact one. Nonetheless, the location of the inclusion is acceptable for all cases. Again, the results in Cases 1, 4 and 6 are practically identical, see also Table 2 for the reconstruction errors, and that Case 5 is slightly inferior. For this example, the current corresponding to the second largest eigenvalue delivers slightly less accurate results although it is still informative, see Table 2.

Acknowledgements

References

[1] Bonesky T, Bredies K, Lorenz DA, Maass P. A generalized conditional gradient method for nonlinear operator equations with sparsity constraints. *Inverse Problems* 2007;23(5): 2041–2058.

[2] Borcea L. Electrical impedance tomography. *Inverse Problems* 2002;18(6): R99–R136.

[3] Bredies K, Lorenz D A, Maass P. A generalized conditional gradient method and its connection to an iterative shrinkage method. *Computational Optimization and Applications* 2009; 42(2): 173–193.

[4] Brühl M, Hanke M. Recent progress in electrical impedance tomography. *Inverse Problems* 2003;19(6): S65–S90.

[5] Cheney M, Isaacson D. Distinguishability in impedance imaging. *IEEE Transactions on Biomedical Engineering* 1992;39(8): 852–860.

[6] Cheney M, Isaacson D, Newell JC. Electrical impedance tomography. *SIAM Review* 1999;41(1): 85–101.

[7] Costabel M. Boundary integral operators on Lipschitz domains: elementary results. *SIAM Journal on Mathematical Analysis* 1988;19(3): 613–626.

[8] Demidenko E, Hartov A, Soni N, Paulsen KD. On optimal current patterns for electrical impedance tomography. *IEEE Transactions on Biomedical Engineering* 2005;52(2): 238–248.

[9] Dobson D C, Santosa F. Resolution and stability analysis of an inverse problem in electrical impedance tomography: dependence on the input current patterns. *SIAM Journal on Applied Mathematics* 1994;54(6): 1542–1560.

[10] Gisser D G, Isaacson D, Newell J C. Electrical current computed tomography and eigenvalues. *SIAM Journal on Applied Mathematics* 1990;50(6): 1623–1634.

[11] Golub G H, van Loan C F. *Matrix Computations*. Johns Hopkins University Press: Baltimore; 1996.

[12] Ito K, Kunisch K. Maximizing robustness in nonlinear ill-posed inverse problems. *SIAM Journal on Control and Optimization* 1995;33(2): 643–666.

[13] Isaacason D. Distinguishability of conductivities by electric current computed tomography. *IEEE Transactions on Medical Imaging* 1986;5(2): 91–95.

[14] Kaipio JP, Seppänen A, Somersalo E, Haario H. Posterior covariance related optimal current patterns in electrical impedance tomography. *Inverse Problems* 2004;20(3): 919–936.

[15] Knowles I. A variational algorithm for electrical impedance tomography. *Inverse Problems* 1998;14(6): 1513–1525.

[16] Knowles I. An optimal current functional for electrical impedance tomography. Preprint, 2004, Department of Mathematics, University of Alabama at Birmingham. Available at `http://www.math.uab.edu/knowles/papers/dnopt.pdf`

[17] Köksal A, Eyüboğlu B M. Determination of optimum injected current patterns in electrical impedance tomography. *Physiological Measurement* 1995;16(3): A99-A109.

[18] Lionheart WR B, Kaipio J, McLeod CN. Generalized optimal current patterns and electrical safety in EIT. *Physiological Measurement* 2001;22(1):85–90.

[19] Lukaschewitsch M, Maass P, Pidcock M. Tikhonov regularization for electrical impedance tomography on unbounded domains. *Inverse Problems* 2003;19(3): 585–610.

[20] Mikhailov S E. About traces, extensions and co-normal derivative operators on Lipschitz domains. In: Constanda C, Potapenko S (eds.) *Integral Methods in Science and Engineering: Techniques and Applications*. Birkhäuser, Boston, 2007: 149–160.

[21] Ramlau R, Teschke G. Tikhonov replacement functionals for iteratively solving nonlinear operator equations. *Inverse Problems* 2005; 21(5): 1571–1592.

Preprint Series DFG-SPP 1324

http://www.dfg-spp1324.de

Reports

[1] R. Ramlau, G. Teschke, and M. Zhariy. A Compressive Landweber Iteration for Solving Ill-Posed Inverse Problems. Preprint 1, DFG-SPP 1324, September 2008.

[2] G. Plonka. The Easy Path Wavelet Transform: A New Adaptive Wavelet Transform for Sparse Representation of Two-dimensional Data. Preprint 2, DFG-SPP 1324, September 2008.

[3] E. Novak and H. Woźniakowski. Optimal Order of Convergence and (In-) Tractability of Multivariate Approximation of Smooth Functions. Preprint 3, DFG-SPP 1324, October 2008.

[4] M. Espig, L. Grasedyck, and W. Hackbusch. Black Box Low Tensor Rank Approximation Using Fibre-Crosses. Preprint 4, DFG-SPP 1324, October 2008.

[5] T. Bonesky, S. Dahlke, P. Maass, and T. Raasch. Adaptive Wavelet Methods and Sparsity Reconstruction for Inverse Heat Conduction Problems. Preprint 5, DFG-SPP 1324, January 2009.

[6] E. Novak and H. Woźniakowski. Approximation of Infinitely Differentiable Multivariate Functions Is Intractable. Preprint 6, DFG-SPP 1324, January 2009.

[7] J. Ma and G. Plonka. A Review of Curvelets and Recent Applications. Preprint 7, DFG-SPP 1324, February 2009.

[8] L. Denis, D. A. Lorenz, and D. Trede. Greedy Solution of Ill-Posed Problems: Error Bounds and Exact Inversion. Preprint 8, DFG-SPP 1324, April 2009.

[9] U. Friedrich. A Two Parameter Generalization of Lions' Nonoverlapping Domain Decomposition Method for Linear Elliptic PDEs. Preprint 9, DFG-SPP 1324, April 2009.

[10] K. Bredies and D. A. Lorenz. Minimization of Non-smooth, Non-convex Functionals by Iterative Thresholding. Preprint 10, DFG-SPP 1324, April 2009.

[11] K. Bredies and D. A. Lorenz. Regularization with Non-convex Separable Constraints. Preprint 11, DFG-SPP 1324, April 2009.

[12] M. Döhler, S. Kunis, and D. Potts. Nonequispaced Hyperbolic Cross Fast Fourier Transform. Preprint 12, DFG-SPP 1324, April 2009.

[13] C. Bender. Dual Pricing of Multi-Exercise Options under Volume Constraints. Preprint 13, DFG-SPP 1324, April 2009.

[14] T. Müller-Gronbach and K. Ritter. Variable Subspace Sampling and Multi-level Algorithms. Preprint 14, DFG-SPP 1324, May 2009.

[15] G. Plonka, S. Tenorth, and A. Iske. Optimally Sparse Image Representation by the Easy Path Wavelet Transform. Preprint 15, DFG-SPP 1324, May 2009.

[16] S. Dahlke, E. Novak, and W. Sickel. Optimal Approximation of Elliptic Problems by Linear and Nonlinear Mappings IV: Errors in L_2 and Other Norms. Preprint 16, DFG-SPP 1324, June 2009.

[17] B. Jin, T. Khan, P. Maass, and M. Pidcock. Function Spaces and Optimal Currents in Impedance Tomography. Preprint 17, DFG-SPP 1324, June 2009.